PAPER

Check for updates

Non-stick performance of polymethylsilsesquioxane thin films synthesized by sol–gel spray coating

Toshiyuki Kajioka, [ID] *[a] Koji Ikegami[a] and Hiromitsu Kozuka [ID] [b]

The non-stick properties of polymethylsilsesquioxane (PMSQ) sol–gel films fabricated *via* spray coating were investigated in this study. A high non-stick performance was achieved by preparing sols under strongly acidic conditions. Infrared absorption spectroscopy analyses suggested that these conditions promoted the formation of highly symmetric Si–O–Si structures, which contributed to the enhanced non-stick behavior. The PMSQ films proposed in this study are transparent and fluorine-free, rendering them suitable for applications such as cooktops.

Introduction

Cooktops are susceptible to burnt-on residues caused by food spills at elevated temperatures. Therefore, imparting non-stick properties to cooktop surfaces is beneficial.

Non-stick coatings containing per- and polyfluoroalkyl substances (PFASs) have been widely used in cookware, such as frying pans. However, in recent years, PFASs have attracted increasing attention and debate because of their potentially harmful effects on the environment and human health.[1–15] In particular, polytetrafluoroethylene reportedly releases toxic gases at high temperatures.[15]

PFAS-free approaches have been explored in various fields. For liquid repellency, strategies such as microstructured[16–21] or liquid-like[21–24] surfaces have been proposed. In non-stick coatings, silica-based organic–inorganic hybrid coatings have been proposed.[25–29] They are often marketed as non-stick "ceramic coatings".[25–27] These coatings consist of silica particles embedded in a siloxane matrix containing Si–CH$_3$ groups. However, the coatings tend to become hazy, which limits design flexibility. Furthermore, the material preparation process is complex.

Therefore, PFAS-free, heat resistant, transparent, and easily fabricated non-stick coatings are desired. Poly-methylsilsesquioxane (PMSQ) stands out as a candidate material. PMSQ is harmless, transparent, and has a higher heat resistance than most organic polymers. Moreover, its capacity for three-dimensional siloxane cross-linking contributes to its exceptional mechanical and hydrolytic durability,[30] as compared with lower-functionality siloxanes. PMSQ can be easily synthesized *via* the sol–gel method through the hydrolysis and condensation of methyltrialkoxysilane, such as methyl-trimethoxysilane (MTMS) and methyltriethoxysilane (MTES).[30–33]

Numerous studies have examined the properties of PMSQ films. Lee *et al.* proposed low-dielectric-constant coatings synthesized by controlling the molecular weight and micro-structure of MTMS-derived polymers.[34] Urata *et al.* fabricated transparent and smooth PMSQ films from MTES and demonstrated that dynamic oleophobicity was maintained even at a high temperature of 350 °C.[35] Dong *et al.* prepared transparent and smooth PMSQ films from MTMS that exhibited excellent liquid repellency.[36] However, the non-stick properties of PMSQ films have not been investigated, and their application to cooktop surfaces has not been explored.

In this study, PMSQ films were fabricated from MTMS using sol–gel and spray methods and their non-stick properties were evaluated. Cost-effective raw materials, specifically MTMS, hydrochloric acid, ammonia, water, and isopropyl alcohol (IPA), were used, and simple preparation processes were followed. Consequently, this study revealed that hydrolyzing MTMS under stronger acidic conditions results in superior non-stick performance. The fabricated PMSQ films exhibited low haze and high durability, as well as excellent mechanical strength, hydrolytic stability, and oil resistance. These properties indicate their potential applicability not only to cooktops, but also to glass windows for ranges and ovens. The effect of the acidic conditions during hydrolysis on the structure of the resultant PMSQ films was also examined by analyzing their infrared (IR) spectra.

Non-stick performance assessments have traditionally relied on subjective human evaluation of the removability of burnt-on food residue, even when conducted in accordance with the DIN/CEN/TS12983-2 standard. This approach raises concerns regarding the variability in the results, which are operator

[a] Nippon Electric Glass Co., Ltd, 1979 Takatsuki, Takatsuki-cho, Nagahama, Shiga, 529-0241, Japan. E-mail: tkajioka@neg.co.jp

[b] Department of Chemistry and Materials Engineering, Kansai University, 3-3-35 Yamate-cho, Suita, 564-8680, Japan

dependent. Therefore, this study proposes a new method for objectively and reproducibly evaluating the non-stick performance by using image analysis to quantify the area fraction of the burnt-on food residue.

Experimental

Preparation of PMSQ non-stick coatings

Coating solutions A0–3 and B1, whose compositions are detailed in Table 1, were prepared following the procedure outlined in the flowchart in Fig. 1(a).

Solutions A1–3 were prepared *via* an acid-catalyzed process as follows: MTMS was mixed with half of the prescribed amount of IPA, while the remaining half was mixed with H_2O and HCl. Subsequently, the latter was added to the former under magnetic stirring. The mixed solution was stirred for 4 h in a sealed container placed in a water bath maintained at 45 °C (1st step aging), followed by dilution with IPA. During aging, hydrolysis and polycondensation of MTMS proceeded. As shown in Fig. 2, solutions A2 and A3 became cloudy during the 1st step aging. Therefore, after dilution with IPA, solutions A2 and A3 were passed through a syringe filter with a pore size of 0.45 μm to obtain a clear solution. Solution A1 remained clear throughout the aging process.

Solution A0 was prepared by combining MTMS and IPA with a mixture of IPA, H_2O, and HCl in the same manner as solutions A1–A3. For solution A0, the entire amount of IPA was used in this step, and neither aging nor dilution was performed.

Solution B1 was prepared *via* an acid–base two-step catalysis process. Solution B1 was synthesized in the same manner as solutions A1–A3 up to the 1st step aging. After 1st step aging for 1 h, aqueous ammonia was added, and the reaction was further conducted under stirring in a sealed container at 45 °C for 3 h (2nd step aging). The resulting solution was then diluted with IPA. The solution remained transparent throughout the process (Fig. 2(d)).

Three types of substrates were employed, namely, mirror-polished, low-thermal-expansion glass–ceramic plates (N-0, Nippon Electric Glass Co., Ltd), alkali-free glass plates (OA-11, Nippon Electric Glass Co., Ltd) formed *via* the overflow down-draw method, and high-resistivity ($\geq$500 Ω cm) silicon wafers (<100>). Low-thermal-expansion glass–ceramics such as N-0 are commonly used in cooktops.[37]
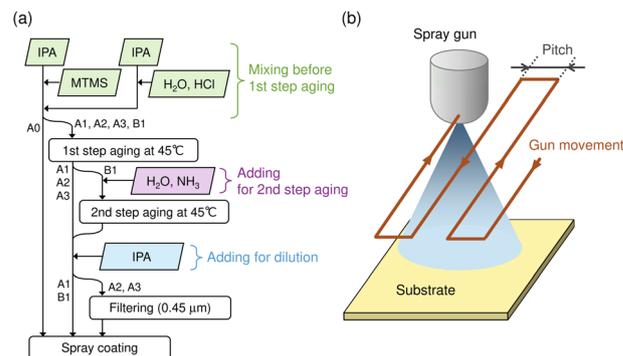

Fig. 1 (a) Flowchart of the solution preparation process. (b) Schematic diagram illustrating the spray gun operation.
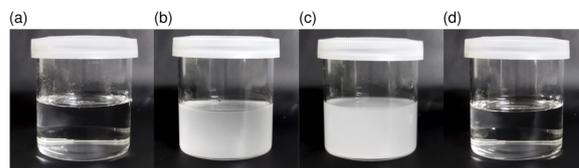

Fig. 2 Appearance of sols (a) A1, (b) A2, (c) A3 and (d) B1 after the aging process.

Prior to coating, each substrate was ultrasonically cleaned for 200 s in water containing 6 wt% of a detergent (SemiClean LGL, Yokohama Oil & Fat Co., Ltd) at 40 °C, followed by rinsing with ultrapure water and subsequent drying.

Spray coating was performed using an in-house externally mixed two-fluid automatic spray gun. As illustrated in Fig. 1(b), the spray gun was positioned perpendicular to the substrate and moved reciprocally at a constant pitch to ensure uniform deposition. The specific spray parameters included a pitch of 5 mm, gun movement speed of 30 m min^{-1}, solution flow rate of 4.6 mL min^{-1}, and atomizing air pressure of 0.2 MPa. After spraying, the deposited PMSQ films were thermally treated in an electric furnace at 350 °C for 30 min for substrates N-0 and OA-11, and at 150, 250, or 350 °C for 30 min for the Si wafers. Hereafter, the N-0 plates coated with solutions A0, A1, A2, A3, and B1, which were primarily used to assess the non-stick properties and related features, are referred to as A0G, A1G, A2G, A3G, and B1G, respectively. The PMSQ-coated OA-11 plates

Table 1 Compositions, aging durations, appearance of the solutions, and resultant sizes of the polymerized species

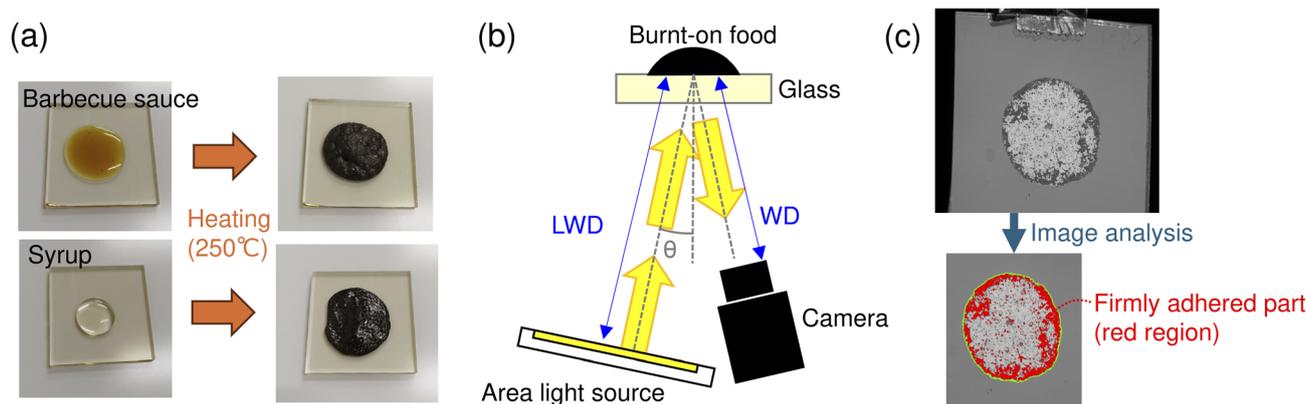| Sol | Molar ratio | | | | | | | Aging duration at 45 °C (h) | | Appearance | Size of polymerized species (nm) |
| | 1st step | | | | 2nd step | | Dilution | | | | |
	MTMS	IPA	H_2O	HCl	H_2O	NH_3	IPA	1st	2nd		
A0	1	108	4	0.002	—	—	—	—	—	Transparent	Off-scale low
A1	1	4	4	0.002	—	—	104	4	—	Transparent	0.86
A2	1	4	4	0.02	—	—	104	4	—	Cloudy	1.09
A3	1	4	4	0.2	—	—	104	4	—	Cloudy	4.22
B1	1	4	3.85	0.002	0.15	0.02	104	1	3	Transparent	2.70

Fig. 3 Evaluation method for non-stick performance. (a) Photographs taken after food dripping and heating. (b) The setup for image capture. The shooting angle was set to $\theta = 4°$, with a working distance (WD) of 350 mm and a light working distance (LWD) of 380 mm. (c) Example of the captured and analyzed image.

were employed solely for haze measurements because their extremely low haze value (<0.01%) enabled a clearer assessment of the film-related haze values, as compared to the uncoated N-0 plates (0.2–0.4%). The PMSQ-coated silicon wafers prepared using solutions A1, A2, A3, and B1 were labelled A1S, A2S, A3S, and B1S, respectively, and were mainly used for measuring the IR absorption spectra.

To study the dependence of film hardness on thickness, PMSQ-coated N-0 plates were prepared by applying larger amounts of solution A3 via smaller coating pitches of 3 and 1 mm, while maintaining all other conditions constant. The samples prepared with the coating pitches of 3 and 1 mm are denoted as A3G′ and A3G″, respectively.

Evaluation of the non-stick performance

Fig. 3 illustrates the procedure for evaluating the non-stick performance. Initially, 0.7 ± 0.1 g of a food ingredient (listed in the next paragraph) was placed on the surface of the sample. The sample was then heated in an electric furnace at 250 °C for 30 min to burn the ingredient (Fig. 3(a)). Next, a photographic image of the sample with burnt-on food was acquired from the rear using a monochrome camera (Fig. 3(b)). Here, the area light source was set to a bright-field arrangement. Based on the image analysis, "the area fraction of the burnt-on food residue" was determined by calculating the total area covered by the burnt food (demarcated in light green in Fig. 3(c)), A_0, and the area where the burnt food adhered to the surface (red in Fig. 3(c)), A_s. The area fraction of the burnt-on residue was then calculated as A_s/A_0. In this analysis, the dark regions, where burnt food was firmly adhered to the surface, and bright regions, where the burnt food detached and floated, were identified using brightness-based thresholding, and A_0 and A_s were calculated based on the pixel count.

Barbecue sauce (Ebara Foods Industry, Inc.) and syrup (SHOEI Co., Ltd) were mainly used as food ingredients. Tomato ketchup (Ikari Sauce Co., Ltd), cake flour (Nisshin Flour Milling, Inc.), and bread flour (Nisshin Flour Milling, Inc.) were also used. A monochrome camera (acA2440-35μm, Basler AG),

a 35 mm focal length lens (VS-3518V, VS Technology Co., Ltd), and an area light source (TREVIEWER, Trytech) were used for image acquisition.

Characterization

The sizes of the MTMS-derived polymerized species in the sol were estimated using a dynamic light-scattering system (Zeta-sizer Nano, Malvern Panalytical). The thickness of the coatings was measured using a stylus profilometer (Dektak XT-S, Bruker Corporation). In this study, the height of the step created by the partial masking of the substrate during spray coating was measured. A haze meter (NDH-5000, Nippon Denshoku Industries Co., Ltd) was used to measure the haze of the coated OA-11 plates. The water contact angle (WCA) was measured using a contact angle meter (DMs-401, Kyowa Interface Science Co., Ltd). The pencil hardness was evaluated according to the ISO 15184 guidelines. Herein, the PMSQ coating was scratched using pencils (Uni, Mitsubishi Pencil Company Ltd) under a load of 750 gf, scratch speed of 0.8 mm s^{-1}, and scratch length of 10 mm. The attenuated total reflection IR (ATR-IR) spectra of the samples were measured using an IR spectrophotometer (Spectrum 3, PerkinElmer) equipped with a ZnSe/diamond prism. The measurement was acquired using 64 accumulations and a resolution of 4 cm^{-1}. The transmission IR spectrum of the PMSQ-coated silicon wafer was measured using an IR spectrophotometer (Frontier FT-IR; PerkinElmer). For this purpose, an uncoated silicon wafer was used as a blank, and the measurement was acquired using 128 accumulations and a resolution of 4 cm^{-1}.

Results and discussion

Thickness, haze, WCA, and non-stick performance of the coatings

Table 2 lists the properties of the coatings obtained. The dynamic contact angles and surface free energies are also provided in SI S.4. All resultant film thicknesses were < 20 nm, ranging from approximately 5 to 17 nm. The thickness of A0G

Table 2 Film thickness, haze, WCA, and area fraction of the burnt-on residue (mean ± standard error)

Sample	Sol	Film thickness (nm)	Haze (%) (OA-11)	WCA (°)	Area fraction of burnt-on residue, $100A_s/A_0$ (%)	
					Barbecue sauce	Syrup
Non-coated glass-ceramic	—	—	0.01 ± 0.00	4.3 ± 0.2	96.0 ± 0.3	44.7 ± 3.6
A0G	A0	4.8 ± 0.6	0.02 ± 0.00	84.4 ± 0.2	21.7 ± 1.4	46.3 ± 1.7
A1G	A1	16.8 ± 1.0	0.14 ± 0.01	90.5 ± 0.2	13.2 ± 3.5	8.8 ± 0.3
A2G	A2	15.2 ± 1.1	0.11 ± 0.01	94.8 ± 0.1	5.4 ± 0.9	4.6 ± 0.6
A3G	A3	16.1 ± 0.7	0.24 ± 0.01	97.4 ± 0.2	2.7 ± 0.1	1.9 ± 0.2
B1G	B1	16.5 ± 1.3	0.46 ± 0.01	93.5 ± 0.3	9.4 ± 0.7	6.9 ± 0.8
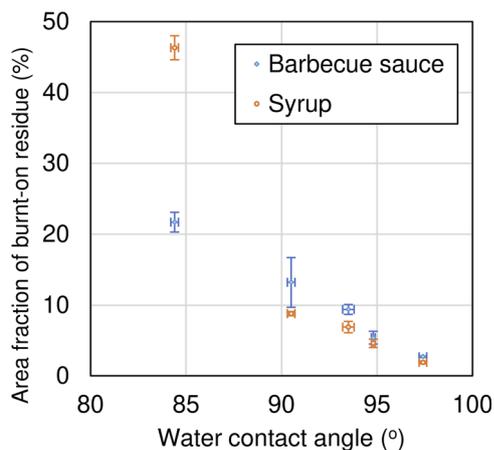
Fig. 4 Relationship between the burnt-on residue area fraction and the WCA.

was smaller than those of the other samples. Because sol A0 was prepared without the aging process that facilitates the hydrolysis and condensation of MTMS, sol A0 was likely rich in volatile monomers and low-molecular-weight oligomers. Therefore, many of the silanes in sol A0 volatilized during spray coating without polymerization to form the coating film.

All the samples exhibited hazes of < 0.5%, and their appearance was clear under normal indoor lighting conditions.

The WCAs were in the order A3G > A2G > B1G > A1G > A0G. For A3G, A2G, and A1G (synthesized under acidic conditions), the increased acidity (Table 1) resulted in higher hydrophobicity. Notably, the hydrophobicity appeared to correlate with the MTMS-derived polymer sizes measured by dynamic light scattering (Table 1). However, the WCA of A2G was higher than that of B1G, although sol B1, synthesized via a two-step acid-base reaction, exhibited a larger polymer size than sol A2. This suggests that factors other than the size of the MTMS-derived polymer play a key role in determining the WCA of the resultant PMSQ coating.

The area fraction of the burnt-on residue for both barbecue sauce and syrup was in the order A3G < A2G < B1G < A1G < A0G. This order was the same as that of the WCA, as shown in Fig. 4 (the relationship between the non-stick performance and hydrophobicity is comprehensively discussed in the subsection "Scorched food sticking mechanism").

Fig. 5 shows images captured after the non-stick performance test. For the samples with PMSQ coatings (b1, c1, d1, e1, f1, b2, c2, d2, e2, and f2 in Fig. 5), the burned portions could be lightly pinched and peeled off with the fingers. The burnt residue firmly adhered to the uncoated glass–ceramic (a1 and a2) and could not be removed with the fingers; they were subsequently scraped off using a stainless-steel scraper. The pattern of the burnt-on areas remaining on the sample surface after removing the burnt food residue (black burnt areas in the rightmost column of the photographs) matched well with the pattern of the areas determined to be stuck by image analysis (red areas in the second column from the right).

A3G, which exhibited the best non-stick performance against barbecue sauce and syrup (Table 2), also possessed excellent performance to other food ingredients, as shown in Fig. 6. In all cases, a higher non-stick performance was achieved, as compared to that of the uncoated N-0 glass-ceramic.

Spray coatings can be easily applied to large areas. A3G fabricated using a relatively large glass–ceramic plate (approximately 140 mm × 200 mm × 4 mm) demonstrated easy removal of burnt tomato ketchup, as shown in the supplementary movie.

Durability of sample A3G

As shown in Table 3, the pencil hardness decreased with an increasing film thickness. Here, the spray application amount of sol A3 increased in the order A3G < A3G′ < A3G″. A pencil hardness greater than 9H was achieved for A3G, which had the smallest thickness.

Table 4 shows that A3G retained its non-stick performance up to 400 °C. After heating at 500 °C, both the WCA and non-stick performance declined. As shown in the ATR-IR spectra in Fig. 7, the absorption peak attributed to Si–CH$_3$ remained after heating at 400 °C, but was not observed after heating at 500 °C, indicating the decomposition of the methyl groups. Furthermore, heat treatment at 500 °C slightly increased the absorption band in the 3000–3400 cm^{-1} region, which corresponds to O–H vibrations. This suggests that Si–CH$_3$ groups are oxidized to Si–OH, which enhances the hydrophilicity of the coatings.

Even after soaking in boiling water or heated oil, no degradation was observed in non-stick performance (Table 4). The WCA slightly decreased after the boiling water test. This phenomenon is attributed to the hydrolysis of Si–O–Si bonds,
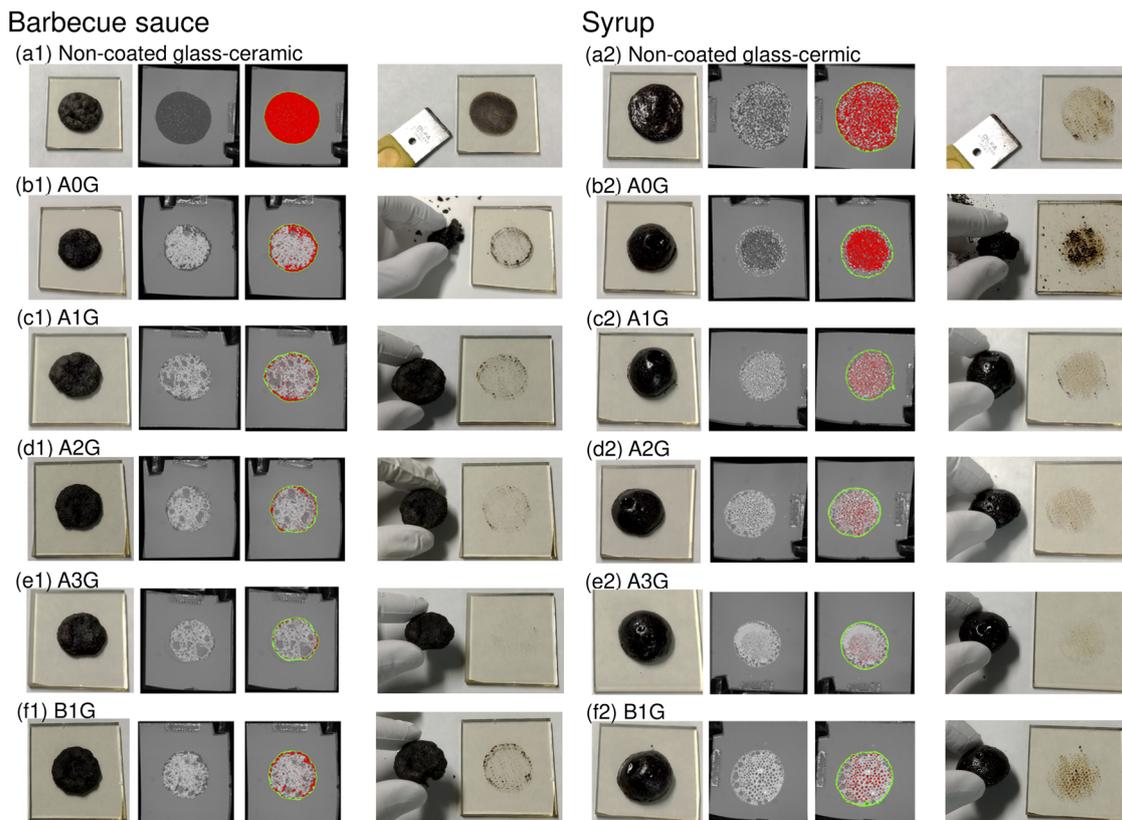
Fig. 5 Sample photographs acquired after the non-stick performance test. The samples and food ingredients used are: (a1) non-coated N-0 plate with barbecue sauce, (b1) A0G with barbecue sauce, (c1) A1G with barbecue sauce, (d1) A2G with barbecue sauce, (e1) A3G with barbecue sauce, (f1) B1G with barbecue sauce, (a2) non-coated N-0 plate with syrup, (b2) A0G with syrup, (c2) A1G with syrup, (d2) A2G with syrup, (e2) A3G with syrup, and (f2) B1G with syrup. For each result, the images from left to right show: a photograph acquired after the burnt-on food was created (left), the image used for analysis, the post-analysis image (with red areas indicating burnt food that is strongly attached and the light green outline demarcating the overall area covered by the burnt food), and the appearance after removal (right).
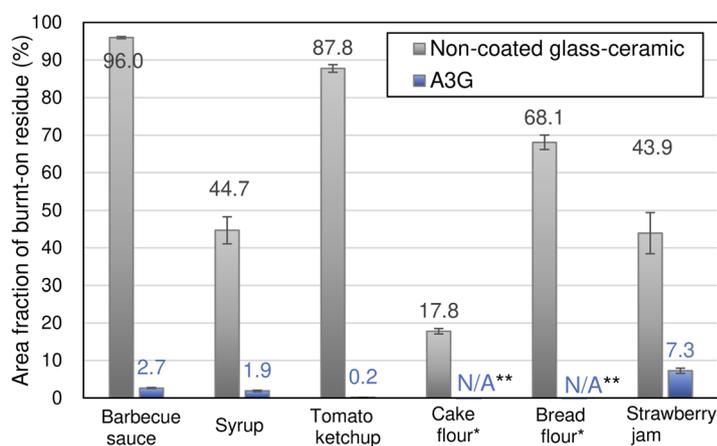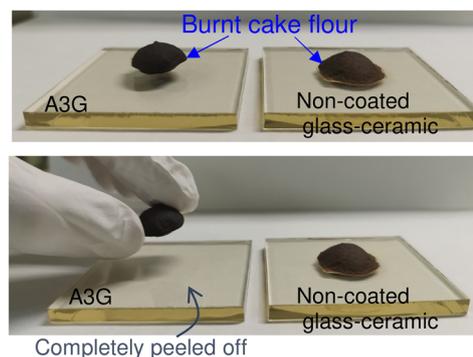
Fig. 6 Results of the non-stick performance tests for A3G with various food ingredients. Cake and bread flour detached completely after heating, making area evaluation impossible (right photographs).

which results in the formation of Si–OH groups on the surface. Following the boiling water test, subsequent heating in air at 250 °C for 30 min restored the WCA to 97.8 ± 0.2°. This recovery is attributed to the recondensation of the surface Si–OH groups.

The high hydrothermal resistance of the PMSQ film is attributed to the synthesis of trifunctional alkoxides, which facilitate the formation of a three-dimensional network of covalent Si–O–Si bonds.[30] In contrast, the WCA of hydrophobic films

Table 3 Film thickness (mean ± standard error) and pencil hardness for A3G, A3G′, and A3G″

|	Film thickness (nm)	Pencil hardness (ISO 15184)
A3G	16.1 ± 0.7	≥9H
A3G′	30.5 ± 2.0	8H
A3G″	74.5 ± 1.5	<7H

fabricated using tetraethyl orthosilicate and monofunctional trimethylchlorosilane (Si(CH₃)₃Cl) significantly decreased after the boiling test, and the WCA remained low even after heating at 250 °C (SI S.2).

No performance degradation was observed after abrasion with a polyurethane sponge soaked in a neutral detergent (Table 4).

Here, we compare our results with the PFAS-free, non-stick coating developed by Ak and Çiçek.[25] They prepared a coating on an aluminum alloy using MTMS, colloidal silica, zirconium propoxide, and polydimethylsiloxane (PDMS), achieving a WCA of 102° and a pencil hardness of 9H by adjusting the Zr/Si ratio and the PDMS content. The hydrophobicity of their coating relies on PDMS, a difunctional siloxane, while neither hydrolytic stability nor heat resistance of the coating was evaluated. The optical clarity of the coating is reported to deteriorate due to its rough surface. In contrast, in the present study, A3G was synthesized *via* the simple hydrolysis and condensation of MTMS, achieving a pencil hardness of 9H along with excellent hydrolytic stability and heat resistance. A3G also demonstrated exceptionally high optical clarity (with a haze value of 0.24%).

Scorched food sticking mechanism

Fig. 8 shows the IR absorption spectra of the burnt-on residues on the bare N-0 surface. Initially, the ATR-IR spectrum of the clean N-0 surface was acquired. Subsequently, each food ingredient was applied, subjected to burning, and scraped off using a clean stainless-steel scraper until the transparent glass–ceramic surface was exposed, followed by the acquisition of the ATR-IR spectrum of the N-0 surface (with a slight amount of burnt-on residue). Differential spectra of the pristine and residue-stuck surfaces were subsequently calculated. Absorptions attributed to the C=O, C–H, and O–H vibrations were observed in the differential spectra, indicating that the burnt residue on the N-0 surface contained these chemical bonds. The –C=O and –OH groups are polar and form hydrogen bonds
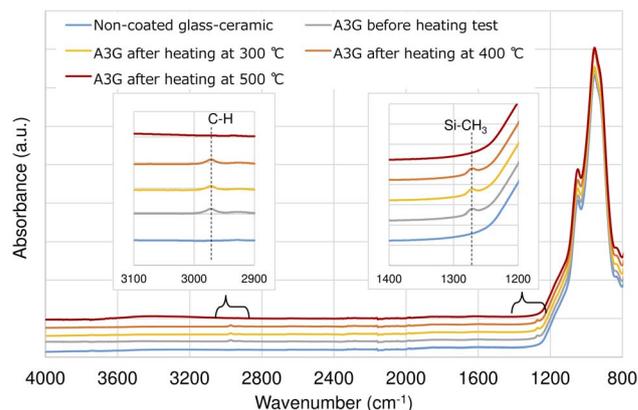
Fig. 7 ATR-IR spectra of A3G before and after the heating tests.

with the Si–OH groups on the glass–ceramic surface, which leads to strong adhesion between the burnt residue and N-0 surface.

In addition to adhesion through hydrogen bonds, the C–OH groups present in the food ingredients were expected to undergo an esterification reaction with the Si–OH groups on the glass–ceramic surface during heating (Si–OH + C–OH → Si–O–C + H₂O). Indeed, Si–OH groups on silica surfaces can reportedly react with the C–OH groups of alcohol *via* esterification at temperatures >100 °C.[38–40]

Although the Si–OH groups on the glass–ceramic surface form hydrogen bonds with the polar groups in the burnt ingredients, the Si–CH₃ groups in the PMSQ film do not. Furthermore, the Si–CH₃ groups are chemically inert and unlikely to react to form covalent bonds. Therefore, the burnt ingredients exhibited poor adhesion to the PMSQ surface. Based on this consideration, larger amounts of Si–CH₃ groups present on the surface are expected to lead to higher WCAs and a better non-stick performance. In fact, Fig. 4 shows a correlation between the WCA and the area fraction of the burnt-on residue.

Factors determining the non-stick properties of PMSQ coatings

As shown in Fig. 4, the PMSQ films with higher WCAs exhibited superior non-stick performances. Furthermore, the PMSQ coatings prepared using sols under strongly acidic conditions

Table 4 Results of durability tests on A3G (mean ± standard error)

	Water contact angle (°)	Area fraction of burnt-on residue (%) (barbecue sauce)
Before test	97.4 ± 0.2	2.7 ± 0.1
Heating (300 °C 3 h)	97.2 ± 0.1	2.4 ± 0.5
Heating (400 °C 3 h)	97.0 ± 0.2	2.6 ± 0.6
Heating (500 °C 3 h)	5.7 ± 0.1	98.5 ± 0.2
Soaking in salad oil (180 °C 1 h)	97.5 ± 0.6	2.1 ± 0.1
Soaking in boiling water (100 °C 1 h)	96.3 ± 0.6	2.9 ± 0.5
Abrasion with a polyurethane sponge[a]	97.3 ± 0.4	2.1 ± 0.5

[a] The polyurethane sponge (WS-77KB, 3M Company) was impregnated with neutral detergent diluted to 5 wt% with water.
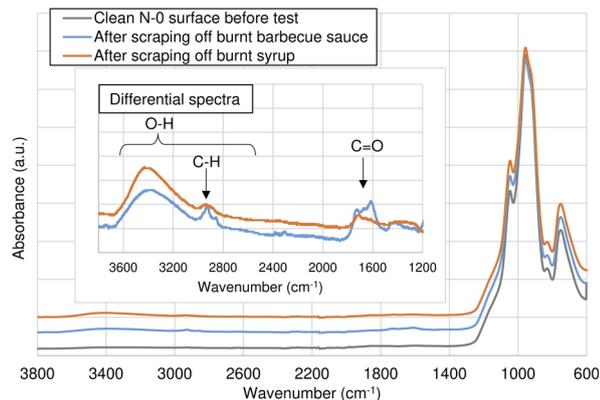
Fig. 8 ATR-IR spectra of the bare glass–ceramic (N-0) surface before and after the food sticking test. The burnt food was scraped off prior to acquisition. The inset shows the differential spectra obtained by subtracting the pre-test data from the post-test.

Fig. 10 Relationship between the WCA and curing temperature for the PMSQ-coated silicon wafers.

exhibited higher WCAs and, consequently, better non-sticking performances.

The WCA is generally determined by surface chemistry and topography.[41,42] All coatings exhibited smooth surfaces with haze values <0.5%, indicating that the contribution of surface roughness to wettability was negligible (for a detailed discussion on surface roughness, refer to SI S.3). Accordingly, the higher WCAs observed for the PMSQ surfaces prepared under strongly acidic conditions were attributed to the increased amount of hydrophobic Si–CH$_3$ groups on the surface, as discussed in the following analysis of the IR absorption spectra.

Fig. 9 shows the IR absorption spectra of the PMSQ-coated silicon wafers A1S, A2S, A3S, and B1S. The spectra were measured after curing at 150, 250, and 350 °C. In the region of 1100–1300 cm^{-1}, the peak intensities at 1030 and 1110 cm^{-1} are labelled as I_L and I_H, respectively. The I_H/I_L ratio decreased with an increasing curing temperature (Fig. 9(e)). Furthermore, at a fixed curing temperature, the samples prepared under more acidic conditions exhibited higher I_H/I_L ratios (A3S > A2S > other samples).

The IR absorption spectrum in the range of 1100–1300 cm^{-1} varies depending on the siloxane structure,[43] which is
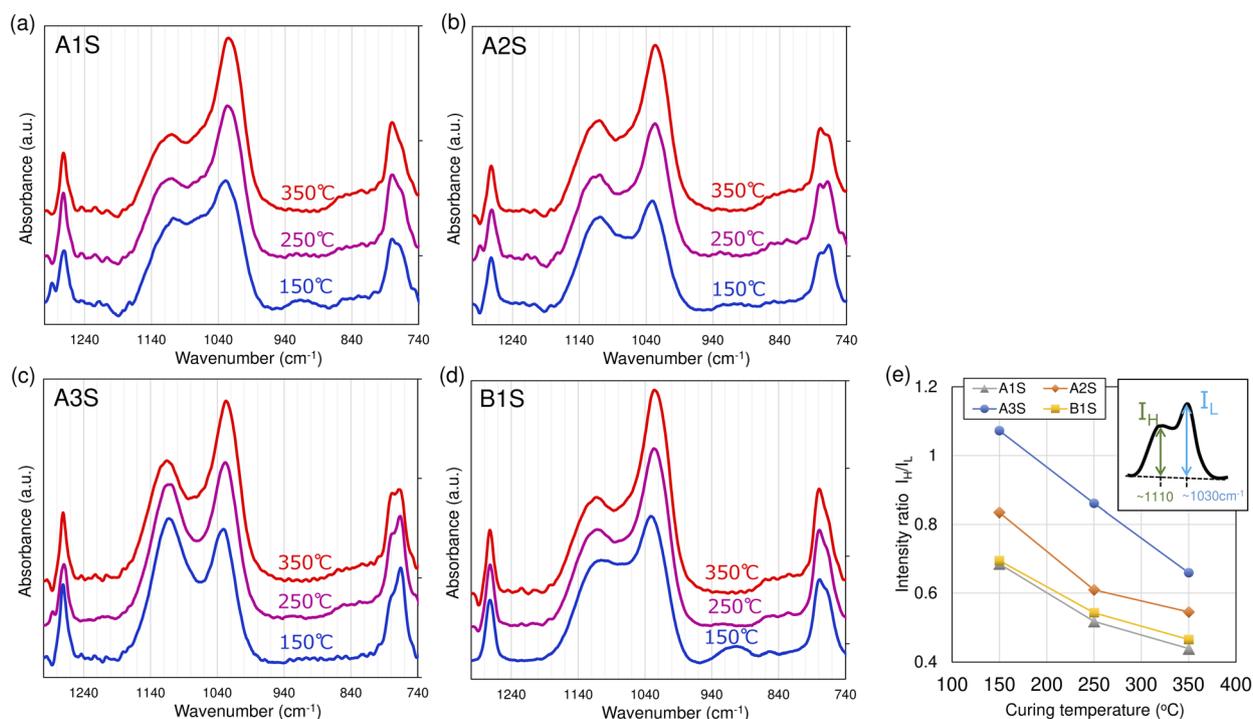

Fig. 9 IR spectra of the PMSQ-coated silicon wafers: (a) A1S, (b) A2S, (c) A3S, and (d) B1S. (e) Relationship between the peak height ratio I_H/I_L (where I_H and I_L are the intensities of the peaks near 1110 and 1030 cm^{-1}, respectively) and the curing temperature. The peak at approximately 1270 cm^{-1} is attributed to Si–CH$_3$ groups, and the absorption in the range of 1100–1300 cm^{-1} is assigned to Si–O–Si groups.

documented for PMSQ in the literature.[44,45] Park *et al.* reported that highly symmetrical structures, such as cages, are IR inactive in the lower wavenumber region.[44] That is, the I_H/I_L ratio increases with the prevalence of highly symmetrical cage-like structures in PMSQ, but tends to decrease in more random structures. The decrease in I_H/I_L with an increasing curing temperature indicates a structural transformation within the siloxane network, likely driven by a thermally induced rearrangement from a highly ordered, symmetric configuration to a more disordered, random structure.

Fig. 10 shows that the WCA increases with an increasing curing temperature. This can be attributed to the reorganization of the siloxane framework accompanied by structural randomization, which promotes the preferential orientation of low-surface-energy Si–CH$_3$ moieties at the film surface. Moreover, the WCA increase is also attributed to the thermal condensation of residual silanol groups (Si–OH + HO–Si → SiO$_2$ + H$_2$O) in the PMSQ matrix. The latter mechanism is supported by the fact that the IR absorption observed at approximately 900–940 cm^{-1} (attributed to Si–OH), which was slightly present after curing at 150 °C, disappeared after high-temperature curing (Fig. 9).

The fact that the higher I_H/I_L ratios were obtained under the stronger acidic synthesis conditions suggests that such conditions promote the formation of PMSQ networks with higher structural symmetry. As shown in Fig. 2, the sols became cloudy during the preparation of sols A2 and A3 (under strongly acidic conditions). This turbidity should result from the abundant formation of cyclic and cage-type siloxanes.[46] Indeed, strongly acidic conditions have been reported to accelerate the formation of cyclic and cage-type siloxanes during the hydrolysis and polycondensation of MTMS and MTES.[46–49]

Even after filtration, the transparent sols A2 and A3 likely contained a significant amount of symmetrical siloxane oligomers, such as cyclic or open-cage types. As shown in Fig. 11, in such siloxane oligomers, Si–CH$_3$ and Si–OH groups are separated and concentrated on opposite sides, in contrast to random-structured siloxanes. Therefore, during film gelation, the surface free energy is minimized by the inward orientation of the Si–OH-rich side and the outward orientation of the Si–CH$_3$-rich side (toward the surface). Consequently, the stronger acidic conditions are expected to lead to a higher proportion of Si–CH$_3$ on the surface during low-temperature curing stage (150 °C). This

is supported by the comparison of the WCAs at 150 °C in Fig. 10, where A3S exhibits the highest value, followed by A2S.

The increase in the curing temperature drives the rearrangement of siloxane and the condensation of Si–OH groups. This combined mechanism increases the proportion of the surface Si–CH$_3$ groups in PMSQ prepared under all catalytic conditions, consequently resulting in an increase in the WCA. However, a higher initial surface concentration of Si–CH$_3$ groups results in a greater retention of Si–CH$_3$ groups, even after high-temperature curing at 250 and 350 °C. Indeed, the order of the WCAs after curing at 150 °C (A3S > A2S > B1S > A1S) was maintained even after curing at 250 and 350 °C.

Conclusions

PMSQ films were fabricated on glass–ceramic plates using a spray coating method based on the hydrolysis and condensation reactions of MTMS, and their non-stick performance was evaluated. Catalytic conditions were varied during the preparation of the coating solutions. Although the sols became cloudy under strongly acidic conditions, filtering the solution before coating yielded transparent PMSQ films. All the fabricated PMSQ films exhibited higher non-stick performances than the uncoated glass ceramic. The non-stick performance of PMSQ was attributed to the Si–CH$_3$ groups on its surface, which effectively prevents the formation of hydrogen and covalent bonds with burnt-food residues. The PMSQ films prepared under strongly acidic conditions exhibited higher WCAs and better non-stick performances. IR absorption spectroscopy revealed that the films prepared under stronger acidic conditions exhibited relatively weaker absorption at approximately 1030 cm^{-1}. This suggests that a strongly acidic condition results in a higher proportion of highly symmetrical siloxane structures, such as open-cage types, which facilitates the formation of PMSQ films with a greater amount of surface Si–CH$_3$ groups during the gelation of films.

Author contributions

T. Kajioka: conceptualization, formal analysis, investigation, visualization, and writing – original draft. K. Ikegami: conceptualization and project administration. H. Kozuka: supervision, writing, review, and editing.

Conflicts of interest

There are no conflicts of interest to declare.

Data availability

The data supporting the findings of this study are available within the article and supplementary information (SI). Supplementary information: materials used for the coating solutions, hydrolytic stability of hydrophobic coatings formed with monofunctional silanes, effect of surface roughness on hydrophobicity and non-stick performance, dynamic contact angles and
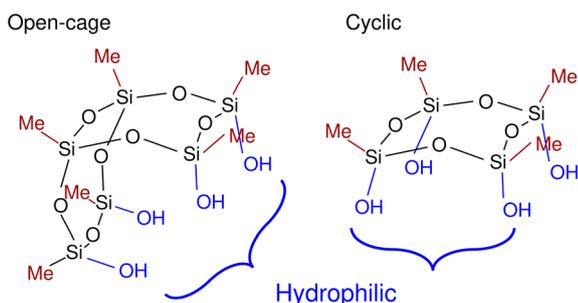

Fig. 11 Open-cage (left) and cyclic (right) methylsilsesquioxane.

surface free energies. See DOI: https://doi.org/10.1039/d5ra08575f.

Acknowledgements

Notes and references

1 S. E. Fenton, A. Ducatman, A. Boobis, J. C. DeWitt, C. Lau, C. Ng, J. S. Smith and S. M. Roberts, *Environ. Toxicol. Chem.*, 2021, **40**, 606–630, DOI: 10.1002/etc.4890.

2 I. T. Cousins, J. C. DeWitt, J. Glüge, G. Goldenman, D. Herzke, R. Lohmann, C. A. Ng, M. Scheringer and Z. Wang, *Environ. Sci.: Processes Impacts*, 2020, **22**, 2307–2312, DOI: 10.1039/D0EM00355G.

3 R. Dhore and G. S. Murthy, *Bioresour. Technol.*, 2021, **341**, 125808, DOI: 10.1016/j.biortech.2021.125808.

4 L. J. L. Espartero, M. Yamada, J. Ford, G. Owens, T. Prow and A. Juhasz, *Environ. Res.*, 2022, **212**, 13431, DOI: 10.1016/j.envres.2022.113431.

5 E. Panieri, K. Baralic, D. Djukic-Cosic, A. B. Djordjevic and L. Saso, *Toxics*, 2022, **10**, 44, DOI: 10.3390/toxics10020044.

6 R. Qu, J. Wang, X. Li, Y. Zhang, T. Yin and P. Yang, *Toxics*, 2024, **12**, 678, DOI: 10.3390/toxics12090678.

7 Z. J. Wen, Y. J. Wei, Y. F. Zhang and Y. F. Zhang, *Arch. Toxicol.*, 2023, **97**, 1195–1245, DOI: 10.1007/s00204-023-03477-5.

8 D. Q. Andrews, T. Stoiber, A. M. Temkin and O. V. Naidenko, *Sci. Total Environ.*, 2023, **901**, 165939, DOI: 10.1016/j.scitotenv.2023.165939.

9 G. T. Ankley, P. Cureton, R. A. Hoke, M. Houde, A. Kumar, J. Kurias, R. Lanno, C. McCarthy, J. Newsted, C. J. Salice, B. E. Sample, M. S. Sepúlveda, J. Steevens and S. Valsecchi, *Environ. Toxicol. Chem.*, 2021, **40**, 564–605, DOI: 10.1002/etc.4869.

10 R. Foguth, M. S. Sepúlveda and J. Cannon, *Toxics*, 2020, **8**, 42, DOI: 10.3390/toxics8020042.

11 T. Ma, C. Ye, T. Wang, X. Li and Y. Luo, *Int. J. Environ. Res. Publ. Health*, 2020, **19**, 16729, DOI: 10.3390/ijerph192416729.

12 T. Ma, X. Pan, T. Wang, X. Li and Y. Luo, *Toxics*, 2023, **11**, 593, DOI: 10.3390/toxics11070593.

13 S. Nayak, G. Sahoo, I. I. Das, A. K. Mohanty, R. Kumar, L. Sahoo and J. K. Sundaray, *Toxics*, 2023, **11**, 543, DOI: 10.3390/toxics11060543.

14 C. Sonne, B. M. Jenssen, J. Rinklebe, S. S. Lam, M. Hansen, R. Bossi, K. Gustavson and R. Dietz, *Sci. Total Environ.*, 2023, **876**, 162770, DOI: 10.1016/j.scitotenv.2023.162770.

15 M. Sajid and M. Ilyas, *Environ. Sci. Pollut. Res.*, 2017, **24**, 23436–23440, DOI: 10.1007/s11356-017-0095-y.

16 S. Shabanian, M. Soltani, S. K. Lahiri, C. Antonini and K. Golovin, *Prog. Mater. Sci.*, 2026, **156**, 101581, DOI: 10.1016/j.pmatsci.2025.101581.

17 K. I. Hegner, C. Hinduja, H.-J. Butt and D. Vollmer, *Nano Lett.*, 2023, **23**, 3116–3121, DOI: 10.1021/acs.nanolett.2c03779.

18 W. S. Y. Wong, M. S. Kiseleva, S. Zhou, M. Junaid, L. Pitkänen and R. H. A. Ras, *Adv. Mater.*, 2023, **35**, 2300306, DOI: 10.1002/adma.202300306.

19 J. Huang, H. Liao, Y. Zhang, W. Wu, M. Wu and X. Gong, *ACS Appl. Mater. Interfaces*, 2025, **17**, 47743–47752, DOI: 10.1021/acsami.5c13258.

20 B. Zhang, W. Wu, G. Yin and X. Gong, *ACS Appl. Mater. Interfaces*, 2025, **17**, 6948–6956, DOI: 10.1021/acsami.4c19137.

21 J. Wassgren and A. Hozumi, *ACS Nano*, 2025, **19**, 27075–27115, DOI: 10.1021/acsnano.5c02443.

22 J. W. Krumpfer and T. J. McCarthy, *Faraday Discuss.*, 2010, **146**, 103–111, DOI: 10.1039/B925045J.

23 I. J. Gresham and C. Neto, *Adv. Colloid Interface Sci.*, 2023, **315**, 102906, DOI: 10.1016/j.cis.2023.102906.

24 X. Cheng, R. Zhao, S. Wang and J. Meng, *Adv. Mater.*, 2024, **36**, 2407315, DOI: 10.1002/adma.202407315.

25 A. Ak and B. Çiçek, *J. Sol-Gel Sci. Technol.*, 2021, **98**, 252–263, DOI: 10.1007/s10971-021-05482-5.

26 A. K. Kumi, A. Chelashaw, Y. M. Zhang and L. F. Li, *Adv. Mater. Res.*, 2012, **622–623**, 420–425, DOI: 10.4028/www.scientific.net/AMR.622-623.420.

27 A. Funayama, *JP Pat.*, JP6170825B2, 2017.

28 M. Sperindio, C. Lake, R. Piras and J. Lindstrom, *US Pat.*, US11193021B2, 2021.

29 S. Lu, J. Shao and F. Wu, *J. Sol-Gel Sci. Technol.*, 2022, **114**, 87–97, DOI: 10.1007/s10971-022-05988-6.

30 R. H. Baney, M. Itoh, A. Sakakibara and T. Suzuki, *Chem. Rev.*, 1995, **95**, 1409–1430, DOI: 10.1021/cr00037a012.

31 C. J. Brinker and G. W. Scherer, Hydrolysis and condensation II: silicates, in *Sol-gel Science*, New York, Academic Press, 1990, pp. 96–233, DOI: 10.1016/B978-0-08-057103-4.50008-8.

32 Y. Abe, H. Hatano and T. Gunji, *J. Polym. Sci., Part A: Polym. Chem.*, 1995, **33**, 751–754, DOI: 10.1002/pola.1995.080330416.

33 N. Takamura, T. Gunji, H. Hatano and Y. Abe, *J. Polym. Sci., Part A: Polym. Chem.*, 1999, **37**, 1017–1026, DOI: 10.1002/(SICI)1099-0518(19990401)37:7<1017::AID-POLA16>3.0.CO;2-F.

34 J. K. Lee, K. Char, H. W. Rhee, H. W. Ro, D. Y. Yoo and D. Y. Yoon, *Polymer*, 2001, **42**, 9085–9089, DOI: 10.1016/S0032-3861(01)00401-3.

35 C. Urata, B. Masheder, D. F. Chenga and A. Hozumi, *Chem. Commun.*, 2013, **49**, 3318–3320, DOI: 10.1039/C3CC41087K.

36 W. Dong, B. Li, J. Wei, N. Tian, W. Liang and J. Zhang, *J. Colloid Interface Sci.*, 2021, **591**, 429–439, DOI: 10.1016/j.jcis.2021.02.014.

37 H. Bach and D. Krause, Glass Ceramics for Household Appliances, in *Low Thermal Expansion Glass Ceramics*, Berlin, Springer, DOI: 10.1007/3-540-28245-9_3.

38 C. C. Ballard, E. C. Broge, R. K. Iler, D. S. St. John and J. R. McWhorter, *J. Phys. Chem.*, 1961, **65**, 20–25, DOI: 10.1021/j100819a007.

39 H. Utsugi, H. Horikoshi and T. Matsuzawa, *J. Colloid Interface Sci.*, 1975, **50**(1), 154–161, DOI: 10.1016/0021-9797(75)90262-3.

40 M. Dion, M. Rapp, N. Rorrer, D. H. Shin, S. M. Martin and W. A. Ducker, *Colloids Surf., A*, 2010, **362**, 65–70, DOI: 10.1016/j.colsurfa.2010.03.044.

41 R. N. Wenzel, *Ind. Eng. Chem.*, 1936, **28**, 988–994, DOI: 10.1021/ie50320a024.

42 A. B. D. Cassie and S. Baxter, *Trans. Faraday Soc.*, 1944, **40**, 546–551, DOI: 10.1039/TF9444000546.

43 P. Innocenzi, *J. Non-Cryst. Solids*, 2003, **316**, 309–319, DOI: 10.1016/S0022-3093(02)01637-X.

44 E. S. Park, H. W. Ro, C. V. Nguyen, R. L. Jaffe and D. Y. Yoon, *Chem. Mater.*, 2008, **20**, 1548–1554, DOI: 10.1021/cm071575z.

45 H. W. Ro, E. S. Park, C. L. Soles and D. Y. Yoon, *Chem. Mater.*, 2010, **22**, 1330–1339, DOI: 10.1021/cm901771y.

46 H. Dong, M. A. Brook and J. D. Brennan, *Chem. Mater.*, 2005, **17**(11), 2807–2816, DOI: 10.1021/cm050271e.

47 H. Dong, M. Lee, R. D. Thomas, Z. Zhang, R. F. Reidy and D. W. Mueller, *J. Sol-Gel Sci. Technol.*, 2003, **28**, 5–14, DOI: 10.1023/A:1025690300105.

48 A. A. Letailleur, F. Ribot, C. Boissière, J. Teisseire, E. Barthel, B. Desmazières, N. Chemin and C. Sanchez, *Chem. Mater.*, 2011, **23**, 5082–5089, DOI: 10.1021/cm202755g.

49 L. H. Lee, W. C. Chen and W. C. Liu, *J. Polym. Sci., Part A: Polym. Chem.*, 2002, **40**, 1560–1571, DOI: 10.1002/pola.10246.